Hindawi
Shock and Vibration
Volume 2020, Article ID 5103261, 10 pages
https://doi.org/10.1155/2020/5103261

Research Article

Numerical Investigation of Performance Improvement and Erosion Characteristics of Vortex Pump Using Particle Model

Daoxing Ye,[1,2] **Hao Li**,[1] **Qiuyan Ma**,[3] **Qibiao Han**,[1] **and Xiulu Sun**[1]

[1]*Farmland Irrigation Research Institute, CAAS/Key Laboratory of Water-Saving Agriculture of Henan Province, Xinxiang 450002, China*
[2]*Key Laboratory of Fluid and Power Machinery, Ministry of Education, Xihua University, Chengdu 610039, China*
[3]*Henan Institute of Science and Technology, Xinxiang 453003, China*

Correspondence should be addressed to Hao Li; leehao.caas@gmail.com and Qiuyan Ma; 15836115756@139.com

Received 14 August 2019; Accepted 18 December 2019; Published 6 March 2020

Academic Editor: M.I. Herreros

Vortex pump has characteristics of low efficiency and serious surface erosion of blade, which seriously affects service life. Therefore, it is particularly important to improve the efficiency of vortex pump and reduce erosion of blade surface. In this investigation, the design of experiment was used to determine the test plan and the number of samples tested. The relationship between geometric factors of vortex pump and efficiency and erosion rate of blade was established using the kriging approximation model. The genetic algorithm solved the multiobjective optimization and obtained the Pareto front solution using NSGA-II. The results showed that the width of nonblade cavity of the vortex pump is reduced by 18.93%, the number of blades of the impeller is increased by one, and the outlet width of the blade is increased by 19.81%. The performance after optimization is significantly improved compared with the original prototype. At design flow rate, the efficiency of the vortex pump increases by 3.24%, while the efficiency increases by 2.59% and 6.24% at $0.8Q_d$ and $1.2Q_d$, respectively. The maximum erosion rate of blade surface 8.52×10^{-4} kg/(m^2·s) is reduced to 7.18×10^{-4} kg/(m^2·s) at $1.0Q_d$ by optimization, which is reduced by 15.73%. The blade erosion after optimization is significantly controlled, and the angle of particle hitting blade surface is reduced.

1. Introduction

Vortex pump (VP) is widely used in agriculture, industry, and wastewater treatment. Due to special structure and working environment, the efficiency of the pump is low, and the surface of flow channel of VP is seriously eroded, which seriously affects service life. Therefore, it is very important to improve performance of VP.

Compared with a general centrifugal pump, the difference of VP is that an impeller is retracted to the rear of volute and the through-flow and circulating flow are formed in impeller and front nonblade cavity when rotating. VP has characteristics of simple structure, easy manufacture, stable operation, good nonblocking performance but large hydraulic loss, low efficiency, and severe blade erosion. At present, Rutschi experimental research showed that an impeller is the main component to determine the performance of VP, and the no-blade width L is an important structural parameter [1]. Most researchers believed that the number of blades increases pump performance, but the number of blades exceeds 9, which has little effect on VP performance. Generally, the number of blades was 6~12 [2]. In terms of pump erosion, Li [3] proposed a flow and wear calculation model for solid-liquid two-phase in a centrifugal pump. For different diameter particles, the Mixture model and DPM model were used, respectively, to introduce the effect of particle volume effect on different volumes. The numerical calculation of solid-liquid two-phase flow of the fraction was carried out, and determining the influence of internal flow of pump on performance and analysis of erosion law were carried out. Zhang used the TE-Wen-Yu model and DC-PDPC model to numerically study a double-

suction centrifugal pump with pumped suspension as main particle containing sand water and established the relationship between sediment concentration and material hardness change and blade wear [4]. Finnie studied the factors affecting metal erosion rate. The results showed that erosion and tear of ductile metals can be quantitatively predicted by hard particle grazing angle impact [5, 6]. Wang Jiaqiong used a particle model and heterogeneous model to numerically simulate the internal flow field of a solid-liquid two-phase centrifugal pump, focusing on the erosion characteristics of wall surface of flow component [7]. Based on the two-phase flow particle orbit model and Tabakoff erosion model, Xianbei numerically simulated a single suction pump to obtain particle trajectory and erosion law under different sediment conditions and different inlet conditions [8]. However, there was no design method that can balance efficiency and erosion rate of the vortex pump. However, the multiobjective optimization design using the nondominated sorting genetic algorithm with the kriging model as the approximate model can obtain ideal results. It has been applied in the multi-objective optimization of centrifugal pump [9–11].

Therefore, in order to improve efficiency of VP and reduce the maximum erosion rate of blade surface as two objectives, the maximum efficiency and the minimum blade erosion rate were used as limiting conditions. The approximate model relationship between hydraulic parameters, erosion rate, and efficiency of VP was established by design of experiment, and then the nondominated sorting genetic algorithm NSGA-II is used to do multiobjective optimization and performance prediction of VP geometry parameters, and finally the comparative study of performance and erosion rate before and after optimization was investigated.

2. Numerical Calculation Method and Erosion Model

For solid-liquid flow, the Eulerian–Eulerian and Eulerian–Lagrangian methods were mainly used for calculation. When the particle diameter is too large, the effect of volume was not be neglected and the Eulerian–Eulerian method had a large error, so the solid particles were calculated as discrete phases, and the liquid phase was still treated as a continuous phase. Due to large diameter of the particles in the vortex pump, the Eulerian–Lagrangian method was used for numerical calculation.

2.1. Governing Equation. A solid-liquid two-phase flow in VP was an incompressible fluid medium, so continuous equation is defined as

$$\frac{\partial \rho}{\partial t} + \frac{\partial \rho\, u_i}{\partial x_i} = 0. \tag{1}$$

The liquid-phase time average governing equation is expressed as

$$\frac{\partial(\rho u \Phi)}{\partial x} + \frac{\partial(\rho u \Phi)}{\partial y} + \frac{\partial(\rho u \Phi)}{\partial z} = \frac{\partial}{\partial x}\left(\Gamma_\Phi \frac{\partial \Phi}{\partial x}\right) + \frac{\partial}{\partial y}\left(\Gamma_\Phi \frac{\partial \Phi}{\partial y}\right) + \frac{\partial}{\partial z}\left(\Gamma_\Phi \frac{\partial \Phi}{\partial z}\right) + S_\Phi + S_{p\Phi}, \tag{2}$$

where u_i is the velocity, x_i is the position, ρ is the density of flow, F is the general variable, and S is the source item.

2.2. Numerical Calculation and Verification. The ANSYS-CFX commercial software platform [12] was used for pump numerical calculation [13–15]. The volute and bladeless cavity domain were set to the stationary coordinate system, and the impeller flow field was rotating coordinate system. The data exchange between rotor and stator was transmitted on interface using the GGI method, and the steady-state calculation was performed using a frozen rotor interface. The solid particles adopt particle transport solid model, and the solid particles were calculated by the Lagrangian method. The distribution of particles was a normal diameter distribution with a diameter of 0.5 mm and a minimum diameter of 0.05 mm. The diameter was 0.25 mm, the standard deviation was 0.07 mm, and the density of solid particles was 2300 kg/m^3. In this article, the Finnie model was used to calculate the erosion characteristic. The rebound coefficient of velocity between solid particle and wall surface was 0.95, and the parallel coefficient was 1. The unidirectional coupling calculation was used between fluid and solid particles, the quality inlet was used for `the calculation domain inlet, and the static pressure of outlet section was set to 0 Pa. All walls were insulated and had no slip wall conditions, and the near wall area used scalable wall function with a wall roughness of 0.05 mm. The residual was 1×10^{-5}. The RNG k-ε turbulence model was used for calculation, and the specific form is

$$\frac{\partial(\rho\varepsilon)}{\partial t} + \frac{\partial}{\partial x_i}(\rho u_i \varepsilon) = -\frac{\partial}{\partial x_i}\left[\left(\mu + \frac{\mu_t}{0.7179}\right)\frac{\partial \varepsilon}{\partial x_i}\right] + \frac{\varepsilon}{k}\left(\left(1.42 - f_\eta\right)P_{\mathrm{k}} - 1.92\rho\varepsilon + \left(1.42 - f_\eta\right)P_{\varepsilon b}\right), \tag{3}$$

$$f_\eta = \eta\frac{(1 - /\eta 4.38)}{(1 + 0.012\eta^3)},$$

$$\eta = \frac{P}{0.085\rho\varepsilon},$$

where $P_{\varepsilon b}$ is the correction factor and P_{k} is the turbulent shear value.

2.3. Erosion Model. Finnie model [6] had advantages of simple formula, less empirical coefficient, and easy calculation, so the Finnie erosion model was used for calculating erosion characteristics of the vortex pump. The erosion of

solid particles and wall of VP was related to the angle of incidence and velocity of particles. Finnie defined the relationship as

$$E = kV_p^n f(\gamma), \tag{4}$$

where E is a dimensionless mass, V_p is the incident velocity of particle, k is a piecewise function related to the incident angle of particle, n is a coefficient between 2.3 and 2.5, and $f(\gamma)$ is defined in formulas (5) and (6) and is shown in Figure 1:

$$f(\gamma) = \frac{1}{3}\cos^2\gamma, \quad \text{if } \tan\gamma > \frac{1}{3}, \tag{5}$$

$$f(\gamma) = \sin(2\gamma) - 3\sin^2\gamma, \quad \text{if } \tan\gamma \le \frac{1}{3}, \tag{6}$$

where γ is the incident angle of particle hitting blade surface. The erosion model consists of two segmentation functions.

Table 1 shows the erosion reference speeds for the different flow wall materials. In the vortex pump, the material of the impeller was wear-resistant steel, and it was hardened steel, so the erosion reference speed was 3321 m/s.

The erosion rate, E_r, of wall surface of VP was defined as

$$E_r = E \times N \times m_p. \tag{7}$$

Erosion rate, E_r, kg/(m^2·s), represents amount of mass reduction per unit area of flow surface, where N is the number of particles per unit time and m_p is the mass of particles.

The ANSYS-ICEM was used to mesh flow fields of the impeller, volute, and vaneless cavity to produce a highly adaptable tetrahedral mesh. Grid independence check [16, 17] was performed using grids of different densities of A, B, C, D, E, and F. The maximum erosion rate and efficiency fluctuation of blade of VP were monitored and are shown in Table 2 and Figure 2. The maximum erosion rate of blade increased with the increase of the number of calculated grids and then gradually stabilized around 8.51×10^{-4} kg/(m^2·s), and η decreased with increasing number of grids and finally stabilized at around 45.9%. The final grid number is 2,381,900.

2.4. Experiment Verification. Comparison of numerical calculation and experiment test is shown in Figure 3. The experiment test was done in a pump enterprise. The details of the setup were marked with serial number as shown in Figure 3. The water and sands (solid particle) were mixed in a tank firstly, and then the mixture was pumped by VP; at last, it came back to the tank.

The performance of numerical calculation and experiment is shown in Figure 4. The comparisons of head and efficiency at flowrate from $0.6Q_d$ to $1.6Q_d$ were studied. As shown in Figure 4, the head calculated by numerical simulation is little higher than which tested by experiment except in $0.6Q_d$ flow condition. The efficiency of VP determined using the numerical method is slightly higher than that measured by using the experimental rig. The overall analysis shows that numerical calculation results agree well with experimental data.

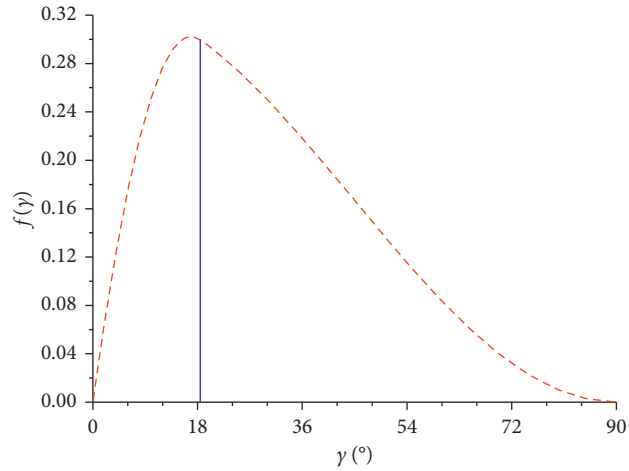

Figure 1: Finnie erosion model.

Table 1: Reference velocity [12].

Wall materials	Reference velocity (m/s)
Aluminum	952
Copper	661
Mild steel	1310
Hardened steel	3321

3. Optimization

3.1. Parameters of Vortex Pump and Blade. The components of VP included a semiopen impeller, a spiral, or annular volute, as shown in Figure 5, wherein Figure 5(a) is an exploded view and Figure 5(b) is blade structure. The diameter of the inlet of VP, D_s, was 50 mm. The diameter of the outlet of the impeller, D_2, was 120 mm. The flowrate, Q_d, was 20 m^3/h, and the head was 16 m. The number of blades was 7, and the outlet of impeller, b_2, was 21 mm. The rotating speed of VP was 2900 r/min.

3.2. Design of Experiment. The chart of optimization process of performance of VP is shown in Figure 6. First, determine optimization target, design variation range of influencing factors, and then use design of experiment (DoE) [18, 19] to determine the experimental scheme and the number of samples, and then use the approximate model. The functional relationship between geometric factors of VP and target was established. After NSGA-II nondominated sorting, the multiobjective optimization of L, b_2, and Z and performance prediction were carried out to find the final target result.

3.2.1. Target of Design of Experiment. The targets of optimization were set to improve efficiency of the pump, reduce the maximum erosion rate of the surface of blade, and propose a multiobjective optimization method for VP, to provide reference for engineering application of product.

Table 2: Grid details.

	Impeller ($\times 10^4$)	Volute ($\times 10^4$)	Total ($\times 10^4$)	Maximum erosion rate E_r (kg/m^{2}s)	Efficiency η (%)
A	68.23	52.31	120.54	7.3160×10^{-4}	49.27
B	93.25	54.26	147.51	7.6744×10^{-4}	48.69
C	103.58	65.72	169.30	8.0664×10^{-4}	47.56
D	112.52	72.91	185.43	8.4373×10^{-4}	47.26
E	125.48	83.56	209.04	8.5124×10^{-4}	45.96
F	140.36	97.83	238.19	8.5113×10^{-4}	45.94

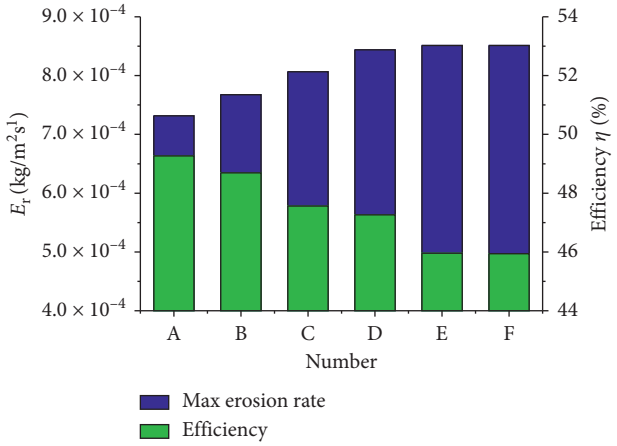

Figure 2: Independency check of the grid.

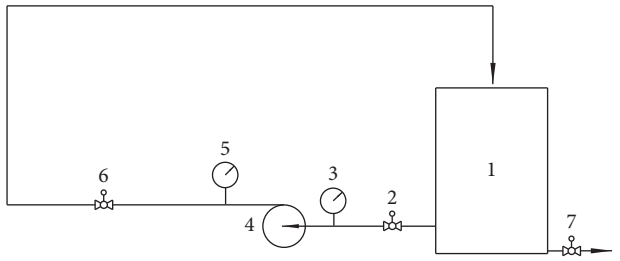

Figure 3: A schematic view of experimental rig. 1: tank. 2: valve. 3: pressure transmitter. 4: vortex pump. 5: pressure transmitter. 6: valve. 7: valve.

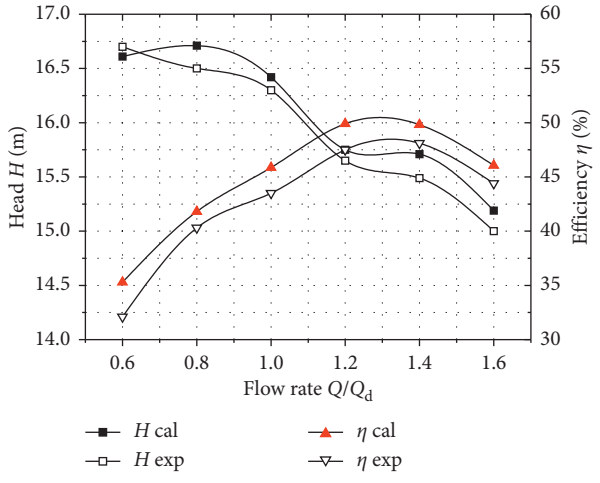

Figure 4: Comparison of calculation and experiment.

3.2.2. Factors and Levels of Design of Experiment. The test sample was arranged using a central composite design (CCD) [19]. The composite design consisted of a factorial design with a central point or a partial factorial design, and it can be enhanced with a set of pivot points to estimate the bend. The factors and level values of test samples are shown in Table 3. L is the width of vane cavity of VP, Z is the number of blades of the impeller, and b_2 is the outlet width of the impeller. According to the prototype size and engineering experience value, level values of factor are shown in Table 3, and the results of sample are shown in Table 4.

3.3. Approximate Model and Optimization Algorithm. The kriging model [18] is an approximate model of unbiased estimator with the smallest estimated variance. The kriging model had characteristics of local estimation, the continuity, and the better conductivity of the correlation function, and it was suitable for solving the problem of high nonlinearity.

The kriging model result was defined as a linear weighted superposition interpolation of the response values. The expression is shown as

$$\hat{y}(x) = \sum_{i=1}^{n} \omega^{(i)} y^{(i)}. \tag{8}$$

By inverting the block matrix, the final kriging model is expressed as

$$\hat{y}(x) = \beta_0 + r^T(x) R^{-1} (y_s - \beta_0 F). \tag{9}$$

The relationship of the maximum erosion rate of blade and efficiency of VP when $L = 30$ mm, $b_2 = 20$ mm, and $Z = 8$ is shown in Figure 7. With increase of cavity width L, the maximum erosion rate of the blade increases first and then decreases as shown in Figure 7(a)). With increase of the number of blades, the maximum erosion rate shows an "M" relationship. E_r decreases first and then increases with the increase of blade width b_2. The efficiency of VP increases with the increase of L, Z, and b_2 as a relationship of increasing first and then decreasing as shown in Figure 7(b), which indicated that the existence of optimal combination of VP makes VP more efficient.

NSGA-II was a multiobjective optimization algorithm based on Pareto optimal solution, which uses the congestion degree and congestion comparison operator and is used as the winning criterion in peer comparison after fast sorting so that individuals in the quasi-Pareto domain can be expanded to the entire Pareto domain, and it maintained diversity of population, introduced the elite strategy, expanded the

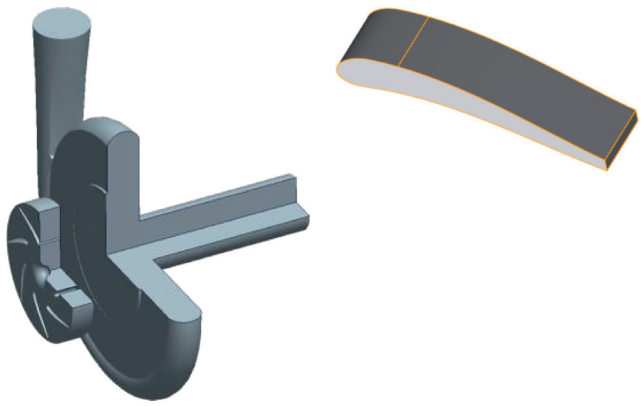

(a) (b)

Figure 5: Structure of the vortex pump and blade: (a) impeller and volute and (b) blade.

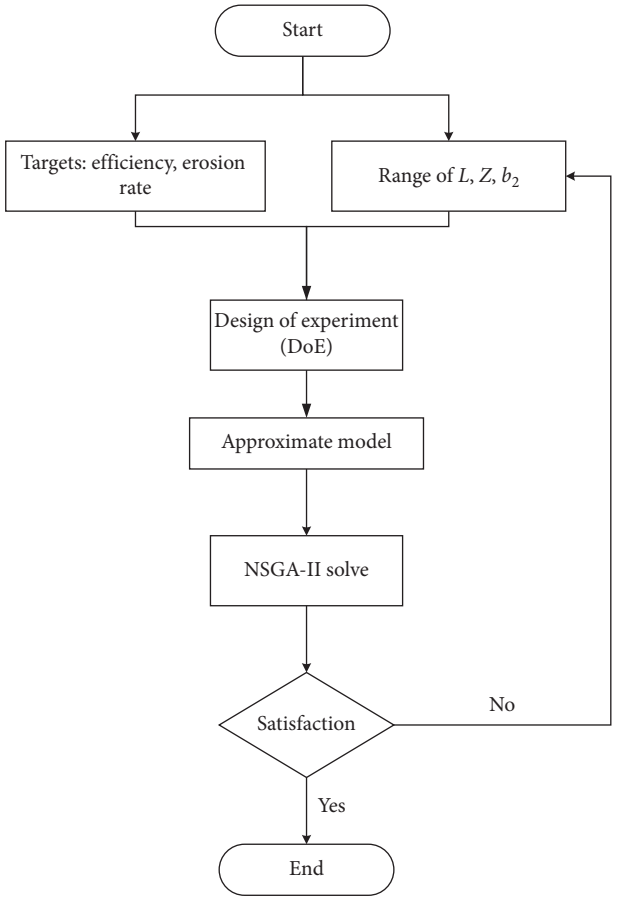

Figure 6: Process of optimization of flow chart.

Table 3: Values of factors and levels.

Level	Factor		
	L (mm)	Z (numbers)	b_2 (mm)
1	20	6	15
2	30	8	20
3	40	10	25

Table 4: DoE of the sample.

Run	L (mm)	Z (numbers)	b_2 (mm)	E_r (kg/(m^2·s))	η (%)
1	40	9	25	0.00071	41.39
2	20	7	25	0.00154	49.72
3	20	7	15	0.00124	46.02
4	40	7	25	0.00089	43.86
5	30	8	20	0.00092	52.39
6	20	9	25	0.00119	48.97
7	30	8	20	0.00095	52.39
8	40	9	15	0.00147	45.29
9	30	8	20	0.00102	52.39
10	30	10	20	0.00084	41.18
11	20	9	15	0.00152	47.12
12	40	7	15	0.00138	44.00
13	46.82	8	20	0.00078	41.53
14	30	6	20	0.00081	46.53
15	30	8	11.59	0.0014	44.04
16	30	8	20	0.00105	52.39
17	30	8	28.41	0.0011	52.71
18	13.18	8	20	0.00083	49.12

sampling space, and improved algorithm's operation speed and robustness. The value of crossover probability was 0.9, mutation probability for real-coded vectors was 1.0, and mutation probability for binary strings was 1.0 in this study. Solution process is shown in Figure 8.

4. Results

The approximation model was solved by the genetic algorithm, and the Pareto frontier was obtained, as shown in Figure 9. The abscissa was maximum efficiency of VP, and the ordinate was maximum erosion rate. The change value of the maximum erosion rate was shown as the color of bubble changed from blue to red. The Pareto front gives the result closest to the design object as shown by the black dotted line in Figure 9. On the Pareto front, the maximum erosion rate of blade of VP decreases with efficiency decreasing.

The geometric parameters before and after the optimization of VP is shown in Table 5. The minimum erosion rate

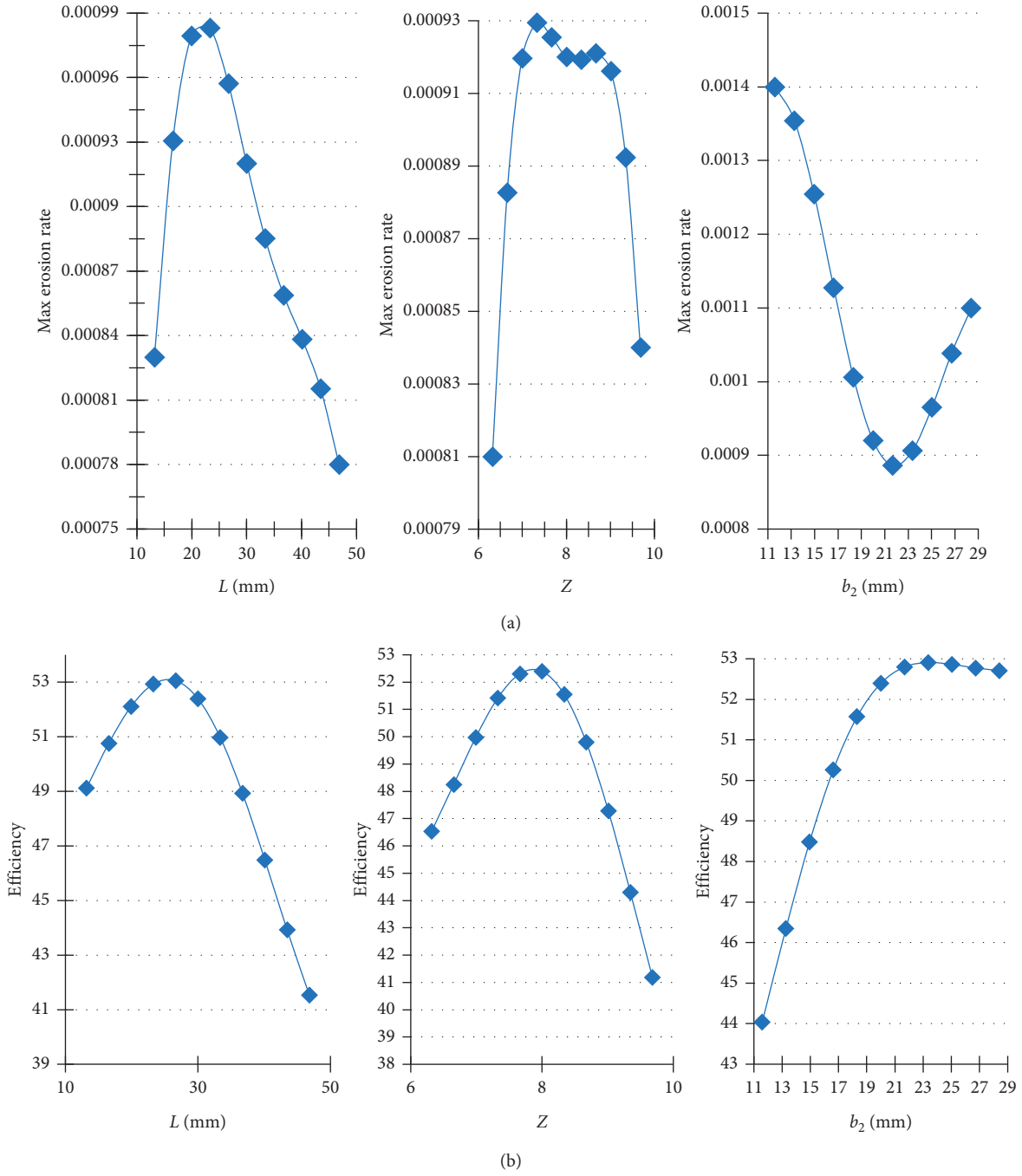

Figure 7: Relationship between objects and factors ($L = 30$ mm, $b_2 = 20$ mm, and $Z = 8$). (a) Maximum erosion rate. (b) Efficiency.

of blade surface and the maximum efficiency of VP were obtained. The optimal parameter combination was obtained by using the NSGA-II algorithm. By comparison, the width of the nonblade cavity of the vortex pump is reduced by 18.93%, the number of blades of the impeller is increased by one, and the outlet width of the impeller is increased by 19.81%.

4.1. Analysis of VP Performance. The comparison chart of head and efficiency of VP before and after optimization is shown in Figure 10. The optimized performance is significantly improved compared with the efficiency of the original prototype. The efficiency of VP is improved by 3.24% at the design flow rate. At $0.8Q_d$ and $1.2Q_d$, the efficiency is increased by 2.59% and 6.24%, respectively. The head of VP is decreased by 5.24% in the design flow rate, and also the head is decreased by 4.01% and 3.43% in $0.8Q_d$ and $1.2Q_d$, which indicates that in the optimization process, a part of head of VP is sacrificed for improving maximum efficiency and decreasing blade erosion rate.

Optimizing the maximum erosion rate of blade surface is significantly reduced as shown in Figure 11. The increase of

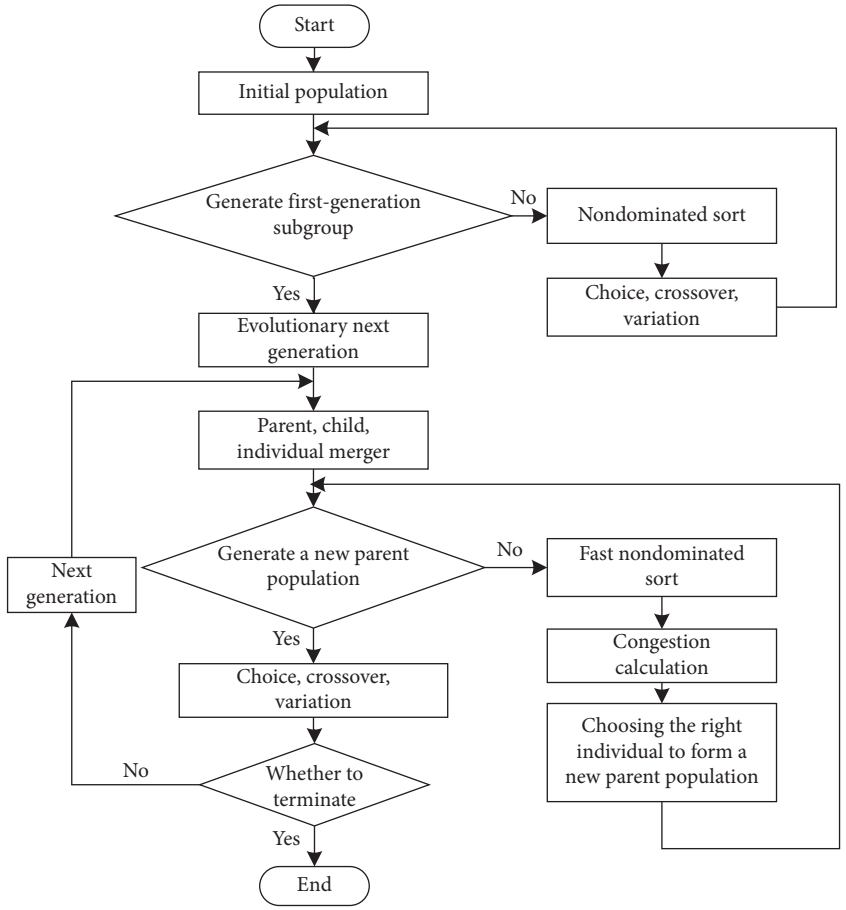

Figure 8: Process of NSGA-II.

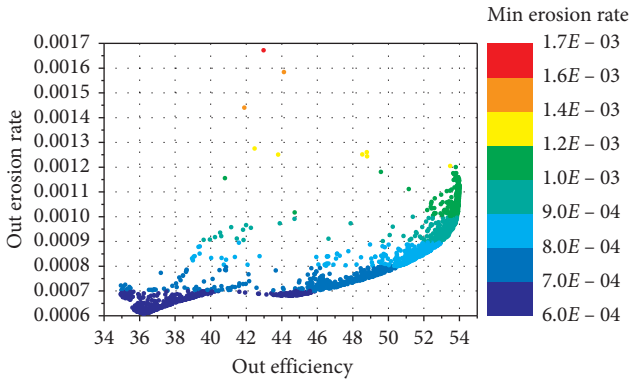

Figure 9: Front of Pareto.

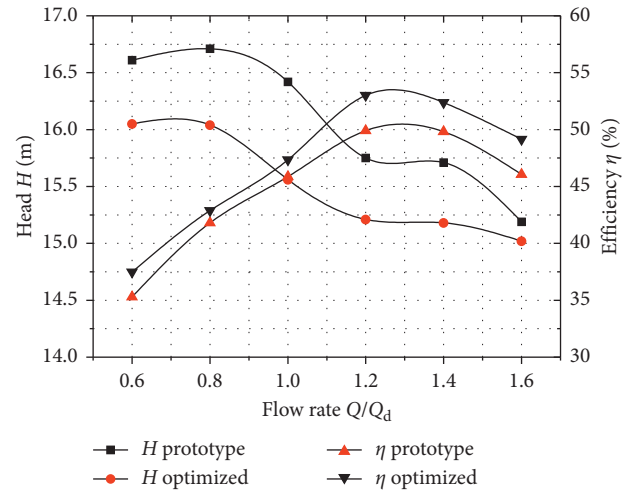

Figure 10: Comparison of performance of the vortex pump before and after optimization.

Table 5: Comparison of geometric parameters before and after optimization.

	L (mm)	Z number	b_2 (mm)
No optimization	30.00	7	21.00
Optimized	24.32	8	25.16

the maximum erosion rate of blade surface corresponds to the increase of the flow rate of VP. The comparative analysis found that the maximum erosion rate of the blade is reduced when the flow rate is more than $1.0Q_d$, and E_r is higher than that before optimization at $0.8Q_d$ and $0.6Q_d$. The maximum erosion rate of the blade, E_r, is reduced from 8.52×10^{-4} kg/(m^2·s) to7.18×10^{-4} kg/(m^2·s) at $1.0Q_d$ condition, which is reduced by 15.73%. The maximum erosion rate increased by 5.86% and 5.86%, respectively, at $0.8Q_d$ and $0.6Q_d$.

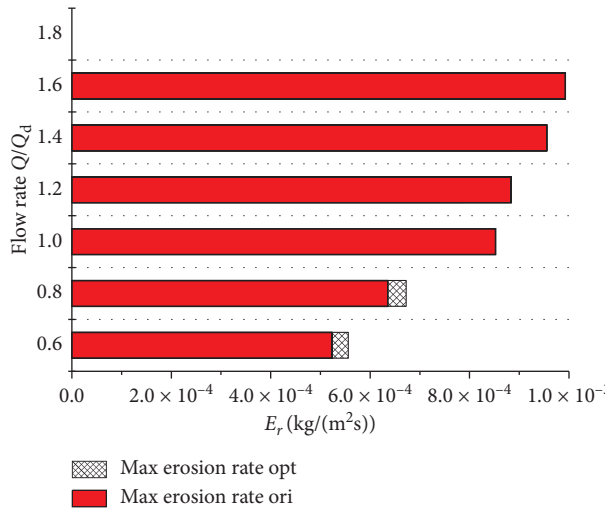

Figure 11: Comparison of average shear stress before and after optimization.

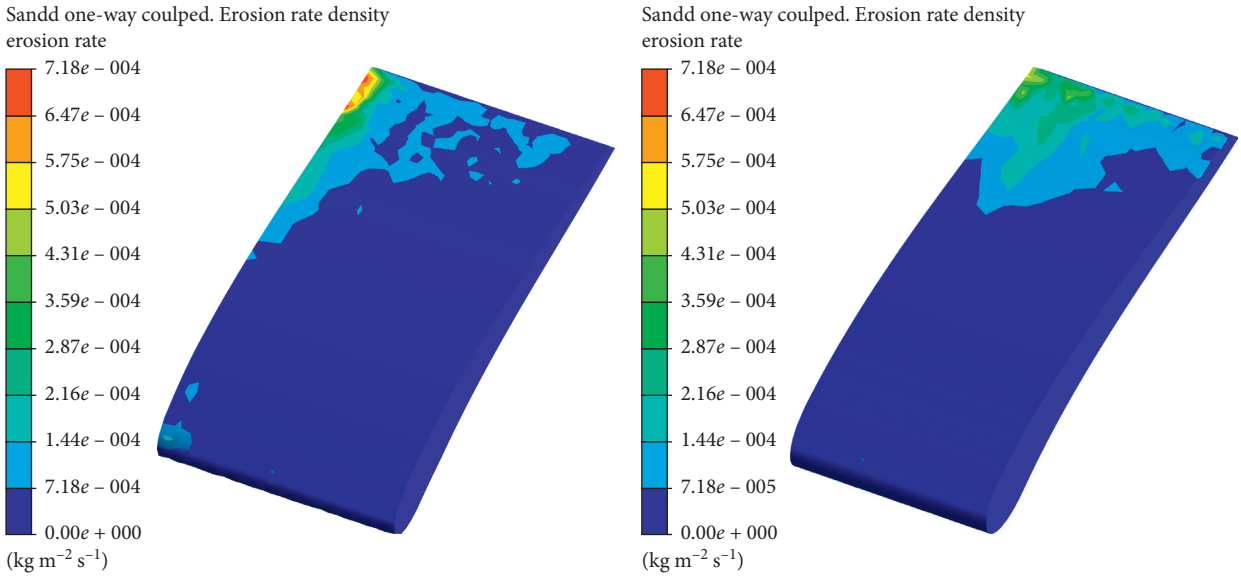

Figure 12: Comparison of erosion rate after optimization. (a) Optimized. (b) Original prototype.

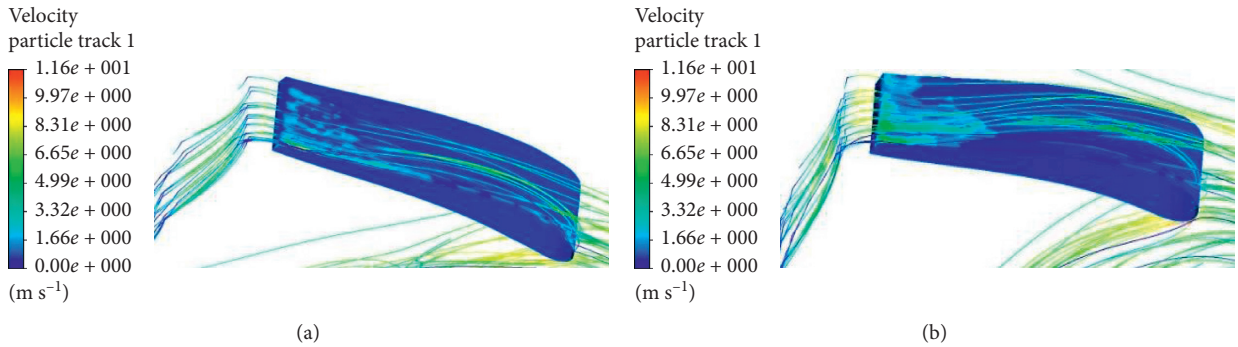

Figure 13: Continued.

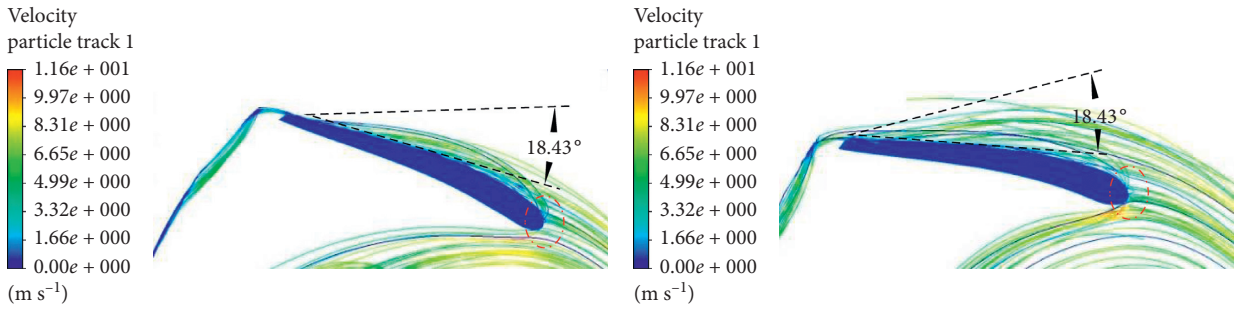

(c) (d)

Figure 13: Comparison of particle motion track after optimization. (a) Optimized. (b) Original prototype. (c) Optimized. (d) Original prototype.

4.2. Erosion Characteristics. The distribution of maximum erosion rate E_r of blade at $1.0Q_d$ is shown in Figure 12, and the distribution at other flow rate was similar. The concentrated area of E_r is near the outlet of the blade. The erosion rate of the blade after optimization is significantly controlled, and the erosion area of the blade is reduced by optimization.

Figure 13 is a comparison of trajectories of solid particles around the blade before and after optimization. After optimization, the trajectory of solid particles flows with VP blade profile as shown in Figures 13(a) and 13(b). The incident angle of particles hitting the blade surface is reduced as shown in Figures 13(c) and 11(d), and the angle as shown is the angle when $\tan\gamma = 1/3$, $\gamma = 18.43^{\circ}$. Some of the solid particles hit the inlet side of blade close to suction side before optimization, which is close to the pressure side after optimization.

5. Conclusions

This paper first designed the optimization goal, then uses the DoE to determine the test plan and the number of samples tested, and then uses the kriging approximation model to establish a functional relationship between VP geometry factor and the efficiency and maximum erosion rate of blade. After NSGA-II nondominated sorting, the multiobjective optimization was solved by using the genetic algorithm, and the Pareto front solution and comparative study were obtained.

After optimization, the width of no-blade cavity, blade width, and number of blades of vortex pump are 24.32 mm, 8, and 25.16 mm, respectively. The width of nonblade cavity of VP is reduced by 18.93%, the number of blades is increased by one, and the outlet width of impeller is increased by 19.81%. The efficiency of VP is improved by 3.24% at the design flow rate. At $0.8Q_d$ and $1.2Q_d$, the efficiency is increased by 2.59% and 6.24%, respectively. The maximum erosion rate of the blade is reduced from 8.52×10^{-4} kg/(m^2·s) to7.18×10^{-4} kg/(m^2·s) at the $1.0Q_d$ condition, which is reduced by 15.73%. The erosion rate of the blade after optimization is significantly controlled, and the erosion area of the blade is reduced by optimization. Some of the solid particles hit the inlet side of blade close to suction side before optimization, which is close to the pressure side after optimization.

Data Availability

The (reference velocity in Table 1) data used to support the findings of this study have been deposited in the help document of ANSYS CFX, Release 17.0.

Conflicts of Interest

The authors declare that they have no conflicts of interest.

Acknowledgments

The support of Central Public-interest Scientific Institution Basal Research Fund (Farmland Irrigation Research Institute, CAAS) (FIRI2018-03), Sichuan Science and Technology Department Plan Project (2019YJ0451), Sichuan Province Department of Education (Grant no. 172467), the Key Project of Xihua University (Grant no. Z1620408), and the Young Scholar Reserve Personnel Project of Xihua University and is gratefully acknowledged. The authors thank their research group for their help.

References

[1] K. Rutschi, "Die arbeitsweise von freistrompumpen," *Schweizerishe Bauzeitung*, vol. 86, pp. 574–582, 1968.

[2] G. P. Schivley and J. L. Dussourd, "An analytical and experimental study of a vortex pump," *Journal of Basic Engineering*, vol. 92, no. 4, pp. 889–900, 1970.

[3] L. Yi, *The Research on Numerical Simulation and Abrasion Property of Solid-Liquid Two-Phase-Flow Centrifugal Pump*, Zhejiang Sci-Tech University, Hangzhou, China, 2014.

[4] Z. Zhang, *Investigation on Sediment Erosion Characteristics of Double Suction Centrifugal Pump*, China Agricultural University, Beijing, China, 2016.

[5] I. Finnie, "Some observations on the erosion of ductile metals," *Wear*, vol. 19, no. 1, pp. 81–90, 1972.

[6] I. Finnie, G. R. Stevick, and J. R. Ridgely, "The influence of impingement angle on the erosion of ductile metals by angular abrasive particles," *Wear*, vol. 152, no. 1, pp. 91–98, 1992.

[7] W. Jiaqiong, J. Wanming, K. Fanyu et al., "Numerical simulation of solid-liquid two-phase turbulent flow and wear

characteristics of centrifugal pump," *Transactions of the Chinese Society for Agricultural Machinery*, vol. 44, no. 11, pp. 53–60, 2013.

[8] H. Xianbei, Y. Shuo, L. Zhuqing et al., "Numerical simulation of erosion prediction in centrifugal pump based on particle track model," *Transactions of the Chinese Society for Agricultural Machinery*, vol. 47, no. 8, pp. 35–41, 2016.

[9] A. Nourbakhsh, H. Safikhani, and S. Derakhshan, "The comparison of multi-objective particle swarm optimization and NASG II algorithm: applications in centrifugal pumps," *Engineering Optimization*, vol. 43, no. 10, pp. 1095–1113, 2011.

[10] Y. Zhang, S. Hu, J. Wu, Y. Zhang, and L. Chen, "Multi-objective optimization of double suction centrifugal pump using Kriging metamodels," *Advances in Engineering Software*, vol. 74, no. 4, pp. 16–26, 2014.

[11] Y. Zhang, S. Hu, J. Wu et al., "Modeling and multi-objective optimization of double suction centrifugal pump based on kriging meta-models," *Advances in Global Optimization*, pp. 251–261, Springer International Publishing, New York, NY, USA, 2015.

[12] ANSYS Inc., *ANSYS CFX, Release 17.0*, ANSYS Inc., Canonsburg, PA, USA, 2017.

[13] F. Zhang, D. Appiah, J. Zhang, S. Yuan, M. K. Osman, and K. Chen, "Transient flow characterization in energy conversion of a side channel pump under different blade suction angles," *Energy*, vol. 161, pp. 635–648, 2018.

[14] F. Zhang, A. Fleder, M. Böhle, and S. Yuan, "Effect of suction side blade profile on the performance of a side channel pump," *Proceedings of the Institution of Mechanical Engineers, Part A: Journal of Power and Energy*, vol. 230, no. 6, pp. 586–597, 2016.

[15] D. Appiah, F. Zhang, S. Yuan, and M. K. Osman, "Effects of the geometrical conditions on the performance of a side channel pump: a review," *International Journal of Energy Research*, vol. 42, no. 2, pp. 416–428, 2018.

[16] H. Chang, W. Shi, and J. W. Liu, "Energy loss analysis of novel self-priming pump based on the entropy production theory," *Journal of Thermal Science*, vol. 28, no. 2, pp. 306–318, 2019.

[17] H. Chang, W. Li, W. Shi et al., "Effect of blade profile with different thickness distribution on the pressure characteristics of novel self-priming pump," *Journal of the Brazilian Society of Mechanical Sciences and Engineering*, vol. 40, no. 11, 2018.

[18] ESTECO Inc., *modeFRONTIER 2016*, ESTECO Inc., Ricerca, Italy, 2016.

[19] X. Zhao, *Experimental Design Method*, Science Press, Beijing, China, 2006.